Assaying the role of complement factor D on retinal pigment epithelial cell pathology in a mouse model of Stargardt disease

By

Xiaoya Xie

A Thesis Submitted in Partial Fulfillment

of the Requirements for the Degree of

BACHELOR OF SCIENCE (HONS).

In the Faculty of Science, Department of Biology

Abstract

Stargardt disease (STGD) is a macular dystrophy caused by mutations in *ABCA4*. *ABCA4* loss-of-function leads to the accumulation of bisretinoids, known as lipofuscin, in the retinal pigment epithelial (RPE) cells in the retina. When photoxidized, lipofuscin can become toxic and cause RPE cell damage as well as activating the complement system of innate immunity. Complement factor D (CFD) is necessary for activating a branch of the complement system called the alternative pathway (AP) and is hypothesized to compromise normal RPE homeostasis which in turns promotes RPE lipofuscin accumulation and photoreceptor degeneration in Stargardt disease. This study examined the process of lipofuscin accumulation over time and how the loss of CFD affects STGD development in 6-month and 12-month *Abca4-/-* mice by quantifying (i) 488 nm RPE autofluorescence as a measure of the accumulation of lipofuscin in paraffin-embedded eye sections, and (ii) the immunofluorescence level of C3 (a critical protein in complement system activation) in the RPE. My results showed that the 488 nm autofluorescence level increased between 6-month and 12-month *Abca4-/-* mice, and between the 12-month *Abca4-/-* and the age-matched wildtype mice. However, the autofluorescence levels were unchanged among the 6-month experimental genotypes. The C3 immunofluorescence level in most of the 6-month experimental genotypes was unchanged. Due to the absence of the disease phenotype (i.e., elevated 488 nm autofluorescence) in the 6-month experimental samples, the role of CFD in STGD progression could not be assessed. Since the results of the autofluorescence assay on paraffin-embedded sections in this study are consistent with what has been observed by others in the Chow lab on flat-mounted RPE, cross-section tissue slides may be used as an alternative for examining the progression of STGD.

Table of Contents

List of figures

Acknowledgments

In this acknowledgment section, I extend my deepest gratitude to all who have walked with me on this journey.

First and foremost, I would like to thank my supervisor, Dr. Bob Chow, for his patience and mentoring. This project would not have been possible without his faith in me.

I thank Dr. Bridget Ryan for selflessly sharing her knowledge with me. Working on a molecular biology-based project as a marine biology student was more challenging than expected, but she made the transition a lot smoother.

I would also like to thank Dr. Barbara Hawkins for all her support as an honour advisor. I know I always have a place to go to when I need guidance navigating this journey.

Thank you to my external examiner, Dr. John Taylor, for all the inspiring questions and valuable feedback.

I am fortunate to have Lauren and Elinor as travel buddies on this journey. We struggled together, but we also supported each other. They made this journey a lifetime memory.

Lastly, I would like to thank my parents. Without their support, I could not make it through this journey.

Chapter 1 Introduction

1. 1 Retina and retinal pigment epithelium layer

The retina is the sensory neuronal component of human eyes. It contains three layers of the retinal neurons with the photoreceptors being the most posterior layer. Two types of photoreceptors are found in the mammalian retina: the rods and the cones. The rod photoreceptors contain rhodopsin and are used for night vision as they are highly sensitive to light. The cone photoreceptors can be further categorized based on their wavelength sensitivity. L type is most sensitive to long wavelength; M type is the cones that are maximally sensitive to the medium wavelength of light; the cone photoreceptors most sensitive to the short wavelength of light are called S type. The combination of different types of cones allows humans to detect colors. The photoreceptor outer segments filled with stacks of folded membranes, outer segment discs, can be found in both the rods and the cones. The visual pigments embedded in the membranes of the outer segment discs contain opsin, a protein, and retinal, a vitamin A-derived chromophore. They are G protein-coupled receptors that will undergo conformational change upon absorption of photons to initiate the phototransduction pathway (Kefalov, 2012; Kolb, 1995). The retinal pigment epithelial layer (RPE) is a monolayer of cells underlying the outer segment layer of the photoreceptors (Figure 1). The macula is the exact center of the posterior portion of the retina. The fovea is located at the center of the macula which contains only cone photoreceptors and is responsible for central vision (Rehman et al., 2024).

The RPE is a single layer of cells posterior to the outer segment layer of the photoreceptors. The apical side of the RPE wraps around the photoreceptor outer segment, and the basal side is highly pleated (Saari, 2012). The RPE is crucial to the health of the retina as it transports nutrients, ions, and water to the photoreceptors. The RPE also protects the retina

against photooxidation by absorbing light. Other functions of the RPE are phagocytosing the shed photoreceptor outer discs, reisomerizing all-*trans*-retinal to 11-*cis*-retinal in the visual cycle, and supporting the integrity of the retina (Simó et al., 2010).

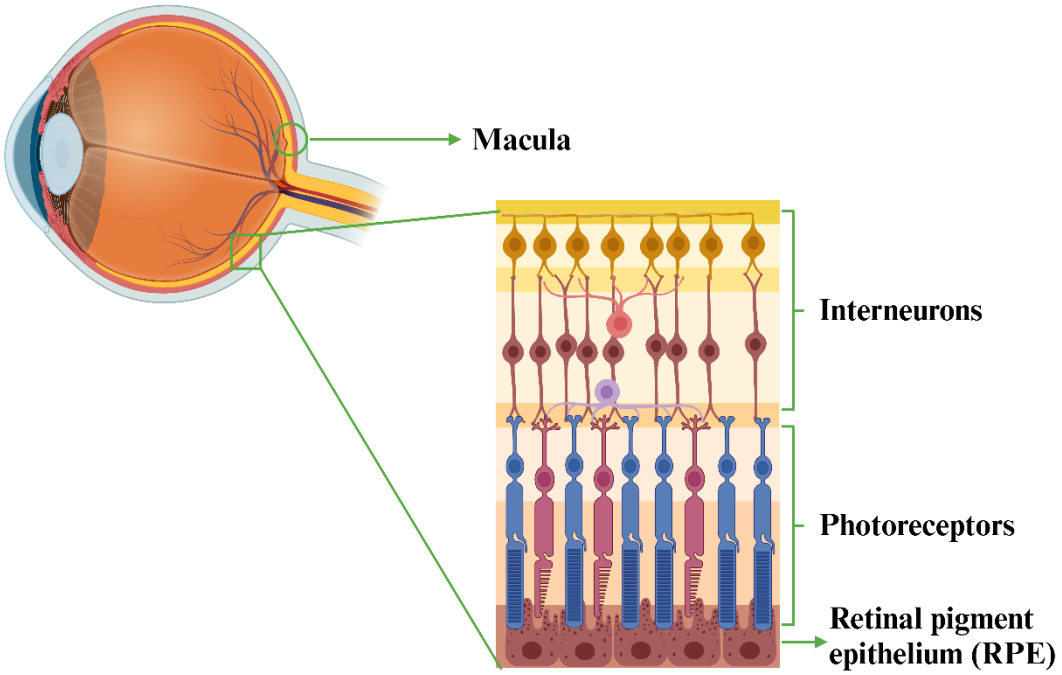

Figure 1. Anatomy of a human eye highlighting the macula and the retina, which includes the photoreceptors (rods and cones) and the monolayer RPE.

1.2 Visual cycle

Phototransduction in photoreceptors is a G-protein-signalling pathway. The visual cycle is activated upon absorption of a photon on the outer segment disc. The opsin-embedded vitamin A-derived chromophore, 11-*cis*-retinal, is then isomerized to all-*trans*-retinal (Scortecci et al., 2021). This transformation activates a GTP-binding protein called transducin. Transducin then hydrolyzes the cyclic GMP-gated channels, leading to the closure of the channels and the hyperpolarization in the outer segment disc. The hyperpolarization eventually reduces the

transmitter (glutamate) released at the synapses, and the visual signals are transmitted to the inner retina for processing and then to the brain (Kolb, 1995; Purves & Williams, 2001). Figure 2 shows multiple processes involving outer segment discs and RPE are required to regenerate 11-*cis*-retinal (Saari, 2012). In the photoreceptor cells, all-*trans*-retinal is reduced to all-*trans*-retinol catalyzed by retinol dehydrogenase (RDH8). The all-*trans*-retinol then diffuses to the RPE where it will be isomerized to 11-*cis*-retinol and converted back to 11-*cis*-retinal via oxidation (Saari, 2012). Interphotoreceptor retinoid-binding protein (IRBP) facilitates the transport of molecules between the outer segment discs and the RPE cells (Perusek & Maeda, 2013).

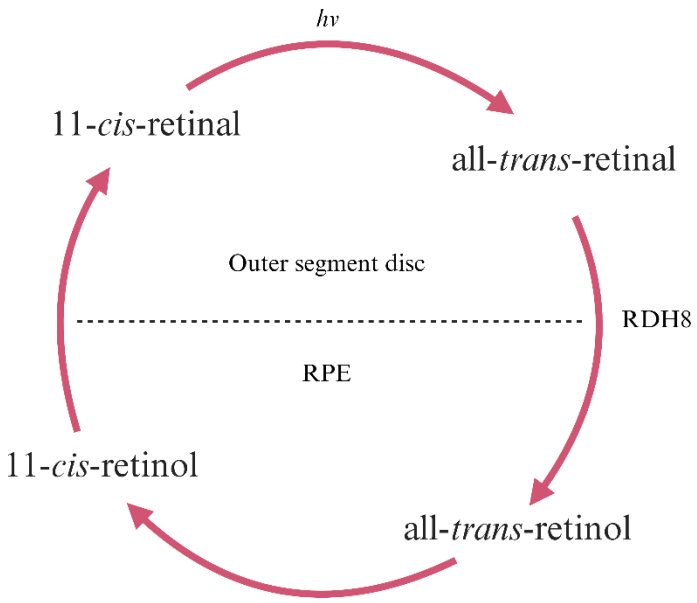

Figure 2. The chemical and conformational transformation of 11-*cis*-retinal in the visual cycle. When the photoreceptor outer disc receives energy from sunlight, the opsin-bound 11-*cis*-retinal- in the membrane will be isomerized to all-*trans*-retinal. The reduction from all-*trans*-retinal to all-*trans*-retinol is catalyzed by RDH8. The isomerization of all-*trans*-retinol to 11-*cis*-retinol happens in the RPE. Lastly, 11-*cis*-retinal is regenerated via the oxidation of 11-*cis*-retinol.

1.3 ABCA4 and its function

After all-*trans*-retinal is released, it binds to phosphatidylethanolamine (PE) and forms N-*trans*-retinylidene-phosphatidylethanolamine (*N*-*t*-ret-PE) (Lenis et al., 2018). Most of the all-*trans*-retinal is released to the cytoplasmic leaflet of the disc membrane, but a small portion may be on the lumenal side. As a result, the head group of *N*-*t*-ret-PE faces either outward into the cytoplasmic space or into the disc lumen. The orientation of *N*-*t*-ret-PE is critical to the progress of the visual cycle because the enzyme RDH8, which is responsible for reducing all-*trans*-retinal, can only be found in the cytoplasm of the outer segment disc. ABCA4, an ATP-dependent transporter located in the outer segment disc membrane as well as the membranes of endolysosomes in RPE, is required to flip the head group of the *N*-*t*-ret-PE to the cytoplasmic side of the membrane so it can undergo isomerization (Figure 3) (Burke et al., 2014; Lenis et al., 2018; Saari, 2012). Mutations in the gene *ABCA4*, which encodes the transporter ABCA4, have been shown to cause autosomal recessive Stargardt disease (STGD) (Allikmets et al., 1997).

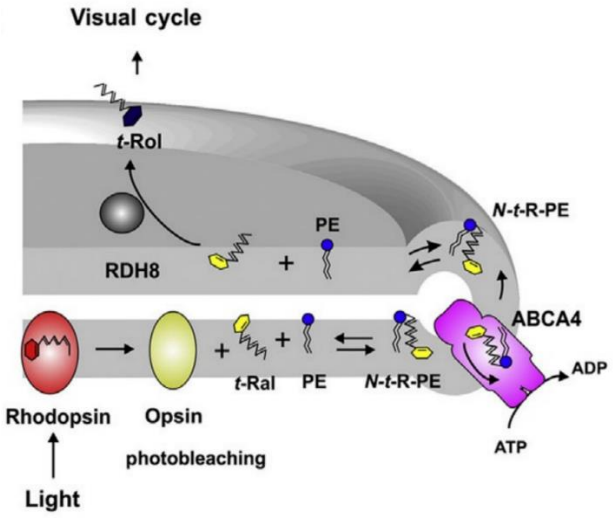

Figure 3. Function of ABCA4 in the visual cycle. When all-*trans*-retinal (*t*-Ral) binds to phosphatidylethanolamine (PE) and forms N- trans-retinylidene-phosphatidylethanolamine (*N*-*t*-R-PE), the head group faces either the cytoplasm or lumen. RDH8 can not reduce *N*-*t*-R-PE if the

head group of *N-t*-R-PE is facing the lumen. ABCA4 flips the complex utilizing ATP so the head group faces the cytoplasmic space for RDH8 to reduce the N-t-R-PE to all-trans-retinol. ABCA4 functions the same in the endolysosomes of the RPE cells (not shown). This figure is adapted from Molday et al., 2022.

1.4 Stargardt disease

Stargardt disease (STGD) is a recessive, heritable form of macular dystrophy that affects 1 in 10,000 people. The symptoms include loss of central vision, which most commonly begins in late childhood or teenage years (Allikmets et al., 1997). The key pathological feature of STGD is the accumulation of lipofuscin in the RPE cells, which is a bisretinoind fluorophore with a maximum excitation at 480 nm (Charbel Issa et al., 2013). Mutations in *ABCA4* lead to the accumulation of *N-t*-ret-PE which undergoes secondary condensation with other *N-t*-ret-PE molecules and forms bisretinoid N-retinylidene-N-retinylethanolamine (A2E) in the outer segment discs (Burke et al., 2014; Charbel Issa et al., 2013). A2E is a major fluorophore of lipofuscin and can potentially activate the complement system (Charbel Issa et al., 2013; Zhou et al., 2006). Lipofuscin is then translocated to the RPE via shedding and phagocytosis of the outer segment discs (Burke et al., 2014). When *ABCA4* is mutated, lipofuscin, namely A2E, will accumulate in the RPE and can be photooxidized by blue light. The accumulation of lipofuscin is thought to increase oxidative stress and activate the complement innate immune system, which consequently affects the RPE cells leading to photoreceptor degeneration in STGD patients (Lenis et al., 2017; Sparrow et al., 2002; Radu et al., 2011).

1.5 Complement system

The complement system makes up part of the innate immune response which is used as an immune defense system throughout the body and in the retina (Xu & Chen, 2016). Activation of the complement pathway can cause inflammation, opsonization, and phagocytosis. It can also

trigger the formation of the membrane attack complex (MAC) and cause cell death. The complement system contains more than 30 proteins which form three pathways: the classical pathway, the lectin pathway, and the alternative pathway (AP). The classical pathway is activated by antigen-antibody complex; the lectin pathway is activated by mannose-binding lectin-associated serine protease (MBL) binding to a pathogen surface; AP is a self-activated pathway through the hydrolysis of C3 component (Boyer et al., 2017; Héja et al., 2012). AP acts as an independent pathway and it also amplifies the classical and the lectin pathways. All three pathways converge at the cleavage of complement factor C3 to C3a and C3b by C3 convertase. After binding to C3b, complement factor B is cleaved into Bb and Ba by CFD forming C3bBb complex. C3bBb complex then forms the second C3 convertase that cleaves more C3 and continues the cascade (Figure 4). The complement cascade is terminated when the C3bBb complex is inactivated in the host cells, or the pathogen cells are lysed by MAC (Boyer et al., 2017). CFD cleaving the hydrolyzed C3 and complement factor B component is thought to be the rate-limiting step in activating the AP and, consequently, the whole complement pathway. Studies also suggested that CFD is required in the initial steps of AP (Barratt & Weitz, 2021; Boyer et al., 2017; H. Xu & Chen, 2016). The accumulation of lipofusin observed in the RPE of *Abca4*-/- mice is thought to trigger the complement system and may lead to the loss of photoreceptor cells as observed in STGD (Charbel Issa et al., 2013; Radu et al., 2011; Wu et al., 2009; Zhou et al., 2006).

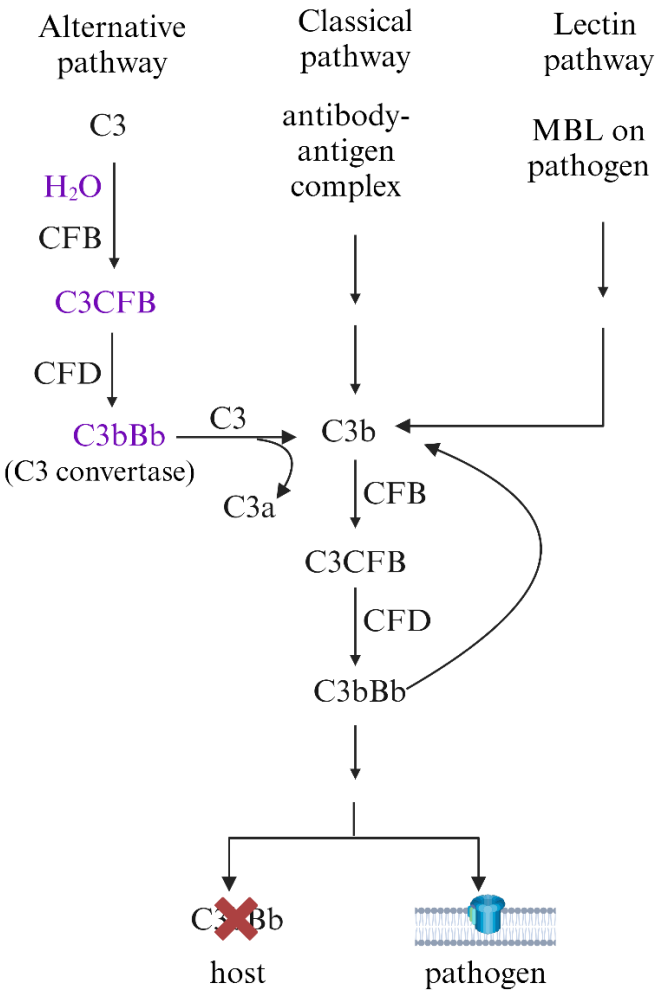

Figure 4. The complement system. It contains three pathways: alternative pathway, classical pathway, and lectin pathway. Purple indicates complexes that contain hydrolized C3. The alternative pathway is a self-activated pathway by hydrolyzing C3. Complement factor B (CFB) then binds to the hydrolyzed C3 and is cleaved to C3bBb by Complement factor D (CFD). C3bBb is a C3 convertase cleaving C3 to C3b and C3a. Activation of the classical pathway by antibody-antigen complex and activation of the lectin pathway by MBL binding to pathogen also lead to the cleavage of C3. C3b then binds to CFB, and the complex is cleaved by CFD to form the second C3 convertase, C3bBb, amplifying the complement cascade. The cascade is terminated when the C3 convertase becomes inactivated in the host cell or when MAC lyses the pathogen cells.

Lenis et al. (2017) attempted to reduce the complement activity in the RPE of *Abca4-/-* mice by increasing the expression of a complement negative regulatory protein (CRP), complement receptor 1-like protein y (CRRY). CRPs inhibit the complement activation which may damage the host cells, namely RPE. The authors hypothesized that the decline in CRPs found in the RPE of mutated mice leads to the elevated activation of the complement system. They overexpressed CRRY by injecting a virus containing the CRRY coding sequence (AAV-CRRY) as a gene therapy. By using gene therapy, i.e., altering the expression level of *CRRY*, the authors showed a normalized complement activity (i.e. a reduction in C3) in the STGD mice. Unexpectedly, they also observed a decrease in lipofuscin deposition and a lower intensity of autofluorescence in the RPE of AAV-*CRRY* injected *Abca4-/-* mice, implying that lipofuscin accumulation had decreased.

1.6 Objectives and hypothesis

Inspired by the study mentioned above, we hypothesized that the progression of STGD pathology is driven by the complement system. Thus, we attempted to reduce the complement activity in STGD mice by crossing them with CFD null mice to generate *Abca4-/-; cfd-/-* double homozygous mice, as another gene therapy for STGD.

To investigate the role CFD plays in STGD, I first examined the amount of lipofuscin in the RPE of different genotypes using autofluorescence intensity quantification as an indicator. Since mutations in *Abca4* slows down the removal of lipofuscin, I hypothesize that the amount of lipofuscin will be larger in the *Abca4-/-* experimental tissue than in other genotypes. I also hypothesize that lipofuscin levels will be greater in the 12-month *Abca4-/-* experimental tissue compared to the 6-month *Abca4-/-* experimental tissue as lipofuscin continues to accumulate in the RPE. Therefore, I predict that the autofluorescence detected in the 12-month *Abca4-*/- mice

will be higher than in the 6-month *Abca4* mutated samples. Finally, based on the findings of Lenis et al. (2017), who observed a decrease in the accumulation of lipofuscin in *Abca4*-/- mice with AAV-CRRY injection, I predict that the autofluorescence level in the *Abca4-/-; Cfd-/-* mice may be lower than the *Abca4* null mice with normal functioning CFD.

Because the loss of CFD can potentially slow down the cleavage of C3, I quantified immunofluorescence intensity as an indirect measurement of the amount of C3 to study the role of CFD in STGD. I hypothesized that because CFD is necessary for AP activation, loss of CFD may delay the complement-driven immune response which is thought to promote STGD disease progression. The immunofluorescence level in the *Abca4* null mice without CFD is predicted to be lower than in the *Abca4* null mice with CFD.

By comparing the autofluorescence results collected using cross-section tissue slides and flat mount, we can determine whether the same trend is observed using cross-section slides. This may provide a more convenient method for studying the roles of different complement factors in STGD using cross-section slides. This study may also provide new insight into how CFD affects STGD at an early stage by examining the C3 content among the experimental genotypes using immunofluorescence.

Chapter 2 Methods and materials

2.1 Mice

The mice used in the experiments are six-month and 12-month pigmented hybrids between strain *129S1* and strain *C57BL/6J* from The Jackson Laboratory. *Abca4-/-* mice (Weng et al., 1999)were crossed with the *Cfd-/-* mice (Xu et al., 2001) to generate *Abca4-/-; Cfd-/-* mice in the subsequent generations, which were used as the model to examine the effect the loss of

CFD has on STGD patients. All work on animals was performed under an approved University of Victoria Animal Use Protocol under the guidelines of the Canadian Council for Animal Care.

2.2 Tissue harvest

The tissue harvest was performed by Bridget Ryan, a post-doctoral fellow in the Chow Lab. The mice were placed in a dark environment for 20 hours before dissection to ensure the tissues were exposed to similar amount of light. The mice were anesthetized by breathing in inhalant isoflurane (AVP, 8061652) and then euthanized via cervical dislocation. The dissection was performed in the dark with dim red light. The eyes were removed using curved forceps. When holding the eyes, a hole was poked using a 27-gauge needle in the nasal side of the eye at the sclera-cornea boundary. The hole marked the nasal side of the eye and let the fixative enter the internal space of the eye. The eyes were transferred into a tube containing fixative made by 4% paraformaldehyde (PFA) and 1x phosphate-buffered saline (PBS) and fixed at room temperature for one hour away from light. They were then washed three times in 1x PBS and transferred into a dish containing 1x PBS for stitching. The suture was performed at the hole poked earlier at the nasal side using a microsurgical needle with suture thread (FST, 12051-08), delicate suture typing forceps (FST, 11063-07), and fine forceps. The stitches marked the correct orientation for paraffin embedding. The eyes were stored individually at 4 °C in a tube filled with 70% ethanol before shipping to Wax-it Histology (Vancouver, Canada) for paraffin embedding. The tissue section was 4 μm thick, cutting through the optic nerve with the dorsal side on the right and the ventral side on the left.

2.3 Deparaffinization, rehydration, and antigen retrieval

Before performing immunolabelling, the paraffin wax on the tissue sections was removed by washing the slides twice in 100% xylenes, followed by rehydration. The tissues were washed twice in 100% ethanol for three minutes each wash, once in 95% ethanol for one minute, one time in 80% ethanol for one minute, and then stored 1x PBS until they were ready for antigen retrieval. I first added 50 mL 1x citrate buffer (10 mM Tri-sodium citrate, 0.5% tween-20, pH 6.0) to each slide chamber and covered the chambers with foil. The tissue slides were added to the chamber once the buffer reached 100 °C and steamed for 30 minutes under 100 °C using a digital steamer (Hamilton Beach, 37530C).

2.4 Nuclei labeling

Although autofluorescence requires no antibody labeling since it is an intrinsic characteristic of lipofuscin, I labeled the nuclei using DAPI to assist in finding the focus when imaging. I incubated the slides used for autofluorescence assay only in 1x PBS with 0.1% triton at room temperature for half an hour to permeabilize the cell membrane after rehydration. The slides were washed three times in 1x PBS after permeabilization. The concentration of the DAPI stock I used was 1mg/ml, and it was diluted in 1:500 dilution factor in 1x PBS and distilled water. After drawing a circle using a PAP pen as a hydrophobic barrier to avoid contamination, I applied 35 µL of DAPI solution to each tissue section. The tissue sections were washed three times with 1x PBS after incubating in a humidified chamber for 30 minutes at room temperature. The slides were mounted with immunomount after.

DAPI labeling was combined with the secondary antibody labeling in the immunolabeling step for slides used for autofluorescence and immunofluorescence assays.

2.5 Immunolabeling

The tissue sections were washed one time in 1x PBS after AR. The primary antibody solution was made by diluting primary antibody stock in 1x PBS containing 0.1% triton with a dilution factor of 1:100. The primary antibody used was rabbit anti-C3 (PAS-21349, Invitrogen) which binds to the alpha chain of C3. I added 120 µL of primary antibody solution onto each slide except the control slides with no primary antibody solution. Instead, I applied 120 µL 1x PBS containing 0.1% triton onto the controls. The tissue sections were incubated in a humidified chamber overnight at 4°C. After overnight incubation, the tissue sections were washed three times in 1x PBS for five minutes each wash. The control slides with no primary antibody solution added were washed separately to avoid contamination.

I used donkey anti-rabbit 647 (A31573, Invitrogen) as the secondary antibody. The secondary antibody stock was diluted in 1x PBS with 0.1% triton by 1:500. I also added 1mg/ml DAPI stock to label the nuclei using the same dilution factor into the secondary antibody stock. The tissue sections were incubated in a humidified chamber at room temperature for 1.5 hours after adding 100 µL of the secondary antibody solution. The slides were washed three times in 1x PBS for five minutes each. I then mounted a coverslip on the tissue section with immunomount. The tissue sections are ready for image collecting after the immunomount is set.

2.6 Image collection

I collected images on two tissue sections per animal. Four images were collected on each section: two immediately dorsal and two immediately ventral to the optical nerve. Autofluorescence was collected using a 488 nm laser, and immunofluorescence was collected using a 640 nm laser. Images were collected using a confocal microscope (Nikon) with 60x objective. The laser power for autofluorescence detection was set to 40 and 20 for immunofluorescence detection. Positive control samples (*Abca4-/-; Rdh8-/-*) were used to determine the optimal gain of each channel. Regions not used for collecting experimental images were used to determine the optimal gain. I recorded the highest possible gain that produced no oversaturated pixels in each image and used the lowest gain to calculate the optimal gain. The optimal gain was two units lower than the lowest gain found using the positive controls. Once the optimal gain was determined for each channel, the condition was applied to all the images collected. Images were collected using the lambda function. If the retina was not on the same field of view as the RPE, i.e., the retina was detached, I collected one image of the retina as the background autofluorescence level. I used the nuclear stain (405 nm channel) to adjust the focus when collecting the experimental images to avoid photobleaching in the autofluorescence and immunofluorescence channels. Because the distribution of laser light on the tissue is not unified, I also collected a uniform green AF image for flat field correction when analyzing the images.

2.7 Quantification

The experimental images were analyzed using image J (FIJI) after being blinded using a custom script. I first defined the region of interest (ROI), namely the RPE, the outer nuclear layer

(ONL), the inner nuclear layer (INL), the nuclei, and the sclera. After the ROIs were defined, I measured the pixel density in the autofluorescence channel and the immunofluorescence channel of each ROI using a customized macro provided by Bridget Ryan. I then averaged the pixel density of the images collected from the same individual. Since other tissues also autofluoresce, background subtraction is needed to measure the autofluorescence emitted by lipofuscin in the general tissue (Croce & Bottiroli, 2014). I averaged the autofluorescence levels in the ONL and the INL of each individual. This background autofluorescence level was subtracted from the total RPE autofluorescence measured in the samples used in the assay that combines autofluorescence and immunofluorescence quantifications. The autofluorescence level of the sclera was subtracted from the total autofluorescence of RPE in the slides used for autofluorescence assay only.

I used C3 knockout mouse as the negative control for immunofluorescence quantification because the immunofluorescence level for C3 is expected to be the lowest since the gene has been knocked out. Because Abca4 functioned normally in the C3 knockout mouse, the autofluorescence level detected in the C3 knockout mouse should be the lowest among all the experimental genotypes. Therefore, it was also used as the negative control for autofluorescence quantification in the experiment which the slides were used for both the autofluorescence and the immunofluorescence quantifications. Another negative control used in the immunofluorescence quantification is *Abca4-/-; Rdh8-/-* with no primary antibody application. In the experiment quantifying the autofluorescence level only, I used the wildtype samples as the negative controls and *Abca4-/-; Rdh8-/-* samples as the positive controls.

2.8 Statistical analysis

Data were presented as mean ± SD. Tukey's Honest Significant Difference (Tukey's HSD) test (R Studio) was performed to analyze the significance of the difference in autofluorescence and immunofluorescence levels between each genotype among the experimental samples.

Chapter 3 Results

3.1 Protocol validation

Before performing my analysis, I wanted to confirm that the procedure used for preparing paraffin-embedded sections for autofluorescence imaging was optimized. I, therefore, examined some of the protocol steps that could potentially influence the levels and quality of 488 nm autofluorescence.

3.1.1 Xylene wash

The residue of paraffin on tissue sections after deparaffinization could potentially interfere with the accuracy of the autofluorescence assay in measuring lipofuscin. Thus, I wanted to test different durations of xylene wash to determine whether residual paraffin affects autofluorescence detection. I performed the following experiment on *Abca4-/-; Rdh8-/-* mice at three and six months of ages.

Examined qualitatively, the brightness of the general tissue was relatively consistent in the merged images of the experimental samples despite the different xylene wash times, namely two minutes, five minutes, 10 minutes, and 15 minutes. However, the autofluorescence image

(Grayscale in Figure 5) with 10-minute xylene wash duration seemed the brightest in the general tissue among the six-month experimental samples (Figure 5).

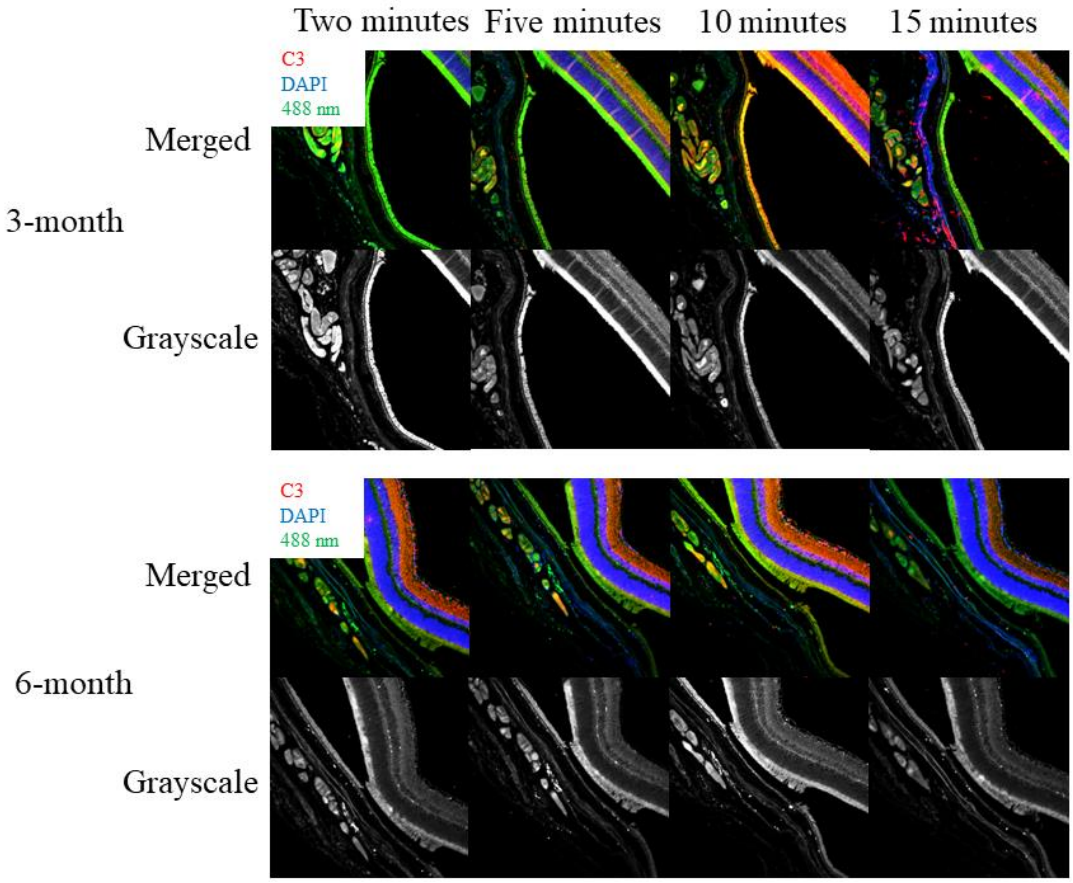

Figure 5. Representative images of autofluorescence and immunofluorescence in the general retinal tissue treated with different xylene wash durations (two minutes, five minutes,10 minutes, and 15 minutes). The images were collected at the inferior region of the retina using 20x objective. In the merged images, the red channel shows C3; the blue channel is nuclei; and the green channel is autofluorescence. Grayscale shows the autofluorescence. The experimental samples are *Abca4-/-; Rdh8-/-* mice at the ages of three months and six months.

When focusing on the RPE, the tissue treated with two-minute xylene wash was the brightest in the merged and autofluorescence images in the 3-month mice samples. The RPE

layer of the slide treated with 10-minute xylene wash duration appeared to be the brightest among the 6-month samples (Figure 6).

Since the tissue treated with five-minute xylene wash did not produce the highest autofluorescence in the experimental tissue, we kept the xylene wash duration at five minutes.

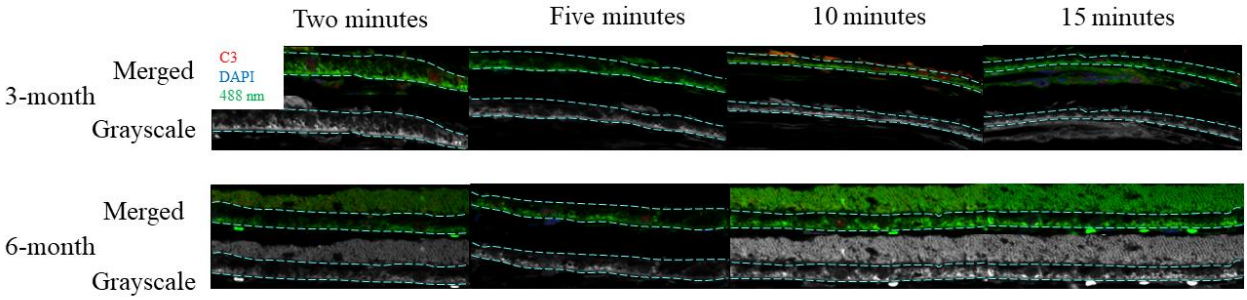

Figure 6. Representative images of autofluorescence and immunofluorescence in the RPE treated with different xylene wash durations (two minutes, five minutes,10 minutes, and 15 minutes). The images were collected at the inferior region of the retina using 60x objective. The dash lines mark the margins of the RPE. In the merged images, the red channel shows C3; the blue channel is nuclei; and the green channel is autofluorescence. Grayscale shows the autofluorescence. The experimental samples are *Abca4-/-; Rdh8-/-* mice at the ages of three months and six months.

3.1.2 Antigen retrieval (AR)

While AR can unmask the immunoactive sites on human tissue, it is also reported to hinder the autofluorescence (Davis et al., 2014; D'Ambra-Cabry et al., 1995). Hence, it is necessary to test how AR affects the autofluorescence detected in the RPE. The experiment I did was quantifying the autofluorescence level in tissue sections with and without AR treatment. The average autofluorescence intensity in the RPE of the *Abca4-/-; Rdh8-/-* samples that underwent AR treatment was 389.34, while the double mutant sample with no AR had an autofluorescence level of 60.25 in the RPE. The wildtype sample with and without AR had autofluorescence intensity of 12.14 and 3.77, respectively, in the RPE.

In terms of variability, the autofluorescence intensity in the RPE of the *Abca4-/-; Rdh8-/-* had a standard deviation of 25.28 which was smaller than the 223.35 calculated in the double mutant samples with no AR treatment. However, an opposite trend was presented in the standard deviation calculated using the wildtype samples: the sample treated with AR had a higher standard deviation than those without (5.85 versus 2.95).

I used the autofluorescence level in the sclera to represent the autofluorescence level in the general tissue. The mean autofluorescence intensity in the *Abca4-/-; Rdh8-/-* samples with AR was 98.62 ± 37.23 and it was 156.64 ± 49.64 in the samples without AR; the wildtype samples had a mean autofluorescence intensity of 9.11 ± 1.36 in the AR samples and autofluorescence intensity detected in the samples without AR was 3.77 ±3.28. Contrasting with the variation in the autofluorescence intensity in the RPE, the double mutant samples with AR had a lower mean and a smaller variation in the general tissue autofluorescence. The mean general tissue autofluorescence intensity was higher in the wildtype samples with AR, 9.11 ± 1.35 versus 3.77 ± 3.28, which agreed with what I observed in the RPE, but the general tissue autofluorescence intensity in the wildtype samples with AR varied less than the ones that did not receive AR.

Although AR amplified the autofluorescence intensity in the RPE in *Abca4-/-; Rdh8-/-* tissues, the effect was minimal among the wildtype samples (Figure 7). To avoid introducing confounding variables, I did not apply AR treatment on the slides used for autofluorescence quantification only.

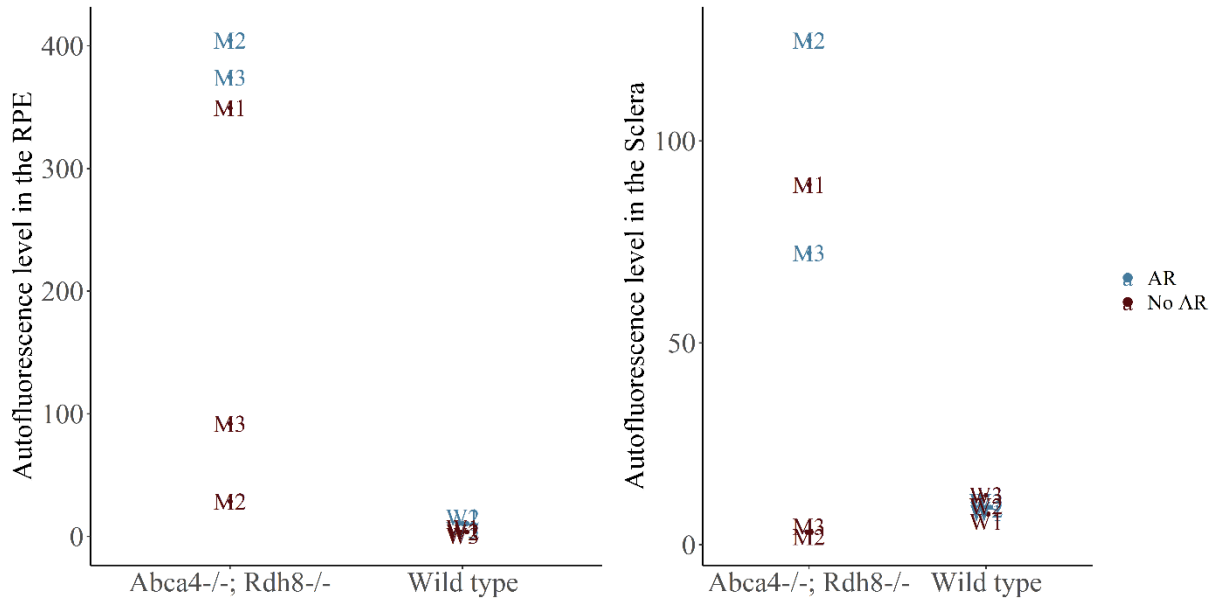

Figure 7. The autofluorescence level in the RPE of *Abca4-/-; Rdh8-/-* and wildtype mice with and without AR (left) and the autofluorescence levels in the sclera of the above genotypes (right). The labels indicate matching individuals. The autofluorescence pixel intensity shown is the mean of eight images collected on the individual, four at the superior and four at the inferior. The autofluorescence in the sclera was used as the background autofluroscence and was subtracted from the total autofluorescence in the RPE. AR has increased the autofluorescence levels in individual M2 and M3 in the RPE and the sclera.

3.1.3 Triton X-100

Solution containing Triton X-100 (Triton for short) has been observed to damage the hydrophobic barrier drawn using PAP pen. In addition, it is unclear whether Triton will introduce confounding variables to the autofluorescence detection. Thus, I examined the integrity of the hydrophobic barrier and the autofluorescence levels between samples to which Triton had or had not been applied. As shown in Figure 8, opposite trends were observed in the RPE autofluorescence levels of the genotype-matched samples. The autofluorescence level in the double mutant with Triton addition was 254.51 higher than in the samples not exposed to Triton.

However, the autofluorescence level detected in the wild type with Triton addition was 49.45 lower than the level detected in the samples without Triton.

The samples treated with Triton had lower immunofluorescence intensity despite their genotype. The immunofluorescence level was 476.71 lower in the double mutant samples with Triton addition, and the wildtype immunofluorescence level was lower by 664.01 when Triton was added to the antibody solution. In addition, the PAP pen circle was damaged when the primary antibody solution contained 0.1% Triton, yet the circle remained intact when Triton was absent in the solution. Based on the result, we excluded Triton from any staining solution to ensure the hydrophobic barrier remained intact during incubation.

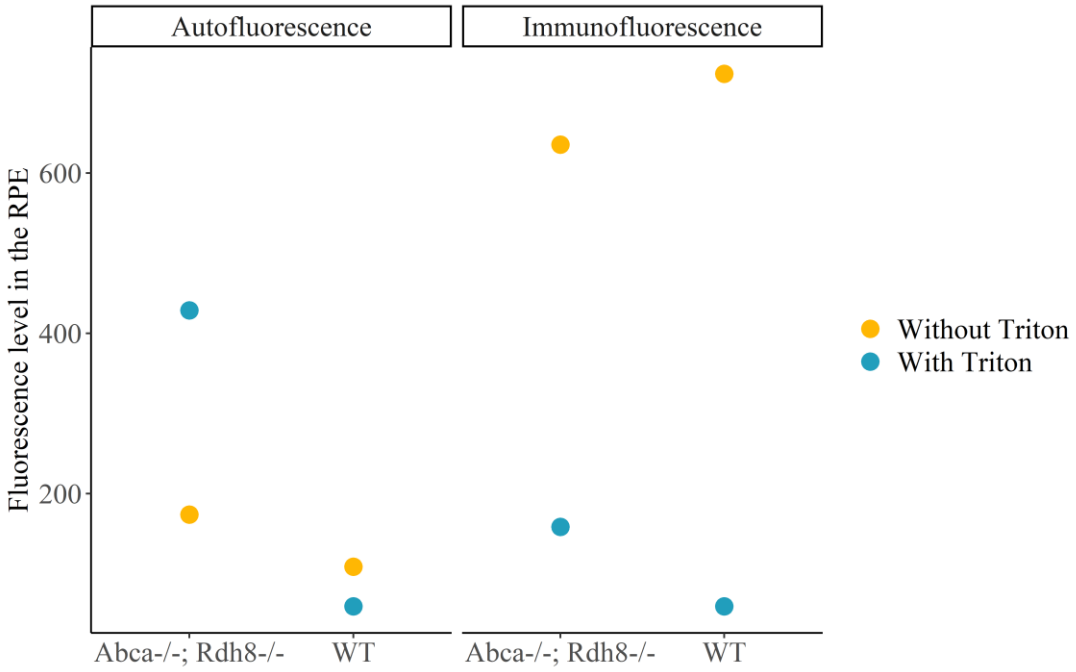

Figure 8. The autofluorescence levels and the immunofluorescence levels between tissue sections applied with solution that either did not contain Triton (blue) or contained Triton (yellow). The x-axis shows the genotypes of the experimental samples. Each dot represents one individual and is the mean fluorescence level calculated using eight images collected. Four images are collected on the superior side of the retina, and four are on the inferior side. Background autofluorescence has been subtracted from the total autofluorescence level of each image.

3.1.4 Nuclei

The number of nuclei found in each image varies, which may cause an overestimation of the immunofluorescence intensity. Hence, I used the control slides to determine whether nuclei should be included in the ROI for immunofluorescence quantification. Immunofluorescence signals were detected in the RPE nuclei of the control samples varying from 86.34 to 1093.94 (Figure 9). The nuclear immunofluorescence varied the most in the images collected using C3 knockout mouse.

Since the nuclear immunofluorescence level can differ significantly among the images collected from the same individual, we excluded nuclei in the ROI to avoid variation caused by this issue.

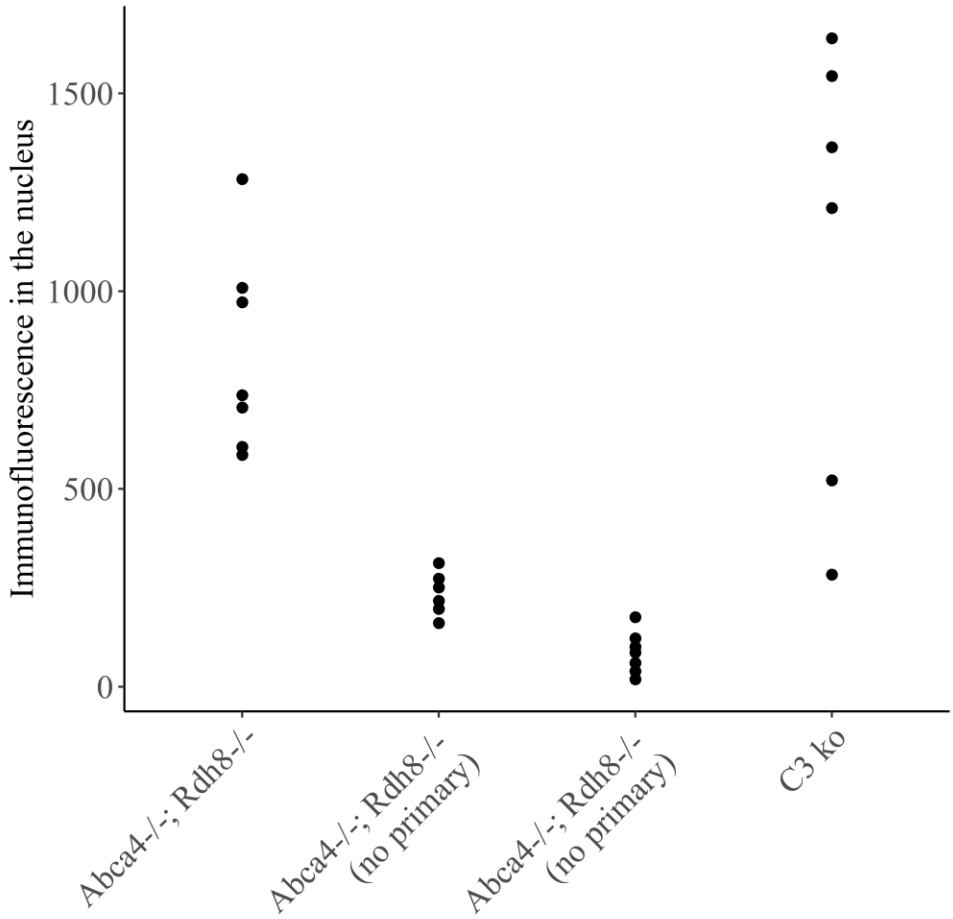

Figure 9. The immunofluorescence levels of the nuclei in the images collected using negative controls. Each point represents an image collected on the tissue sections. The genotypes of the controls are on the x-axis. The nuclear immunofluorescence levels in the two negative control individuals (*Abca4-/-; Rdh8-/-* without primary antibody) are minimal, but the pixel intensity varies significantly in other control slides due to the difference in the number of nuclei contained in the image.

3.2 Autofluorescence

A2E, the main fluorophore found in the lipofuscin, can be measured indirectly using fluorescence microscopy at 488 nm wavelength (Charbel Issa et al., 2013). Thus, I quantified the autofluorescence levels in the RPE of the experimental genotypes to examine the manifestation

of STGD phenotype in *Abca4* null mice. The wildtype had an average autofluorescence level of 14.05 ± 120.08, and the mean autofluorescence level in the RPE of the *Cfd-/-* samples was -60.66 ± 134.03 in the samples with C3 labeling. The mean autofluorescence level for *Abca4-/-* and *Abca4-/-; Cfd-/-* were -43.81 ± 136.27 and -4.51 ± 62.03, respectively. As shown in Figure 10A, the lowest autofluorescence intensity among the experimental samples, -348.80, was found in *Abca4-/-* and the highest autofluorescence intensity of all experimental samples was observed in a wildtype sample, being 341.83.

In the samples with no C3 labeling, meaning no AR or application of Triton, the six-month wildtype had an autofluorescence level of 0.52 ± 55.62, with a maximum of 67.44 and a minimum of -56.16. The mean autofluorescence level in the RPE of the six-month *Abca4-/-* samples was 34.95 ± 32.95 with a maximum of 61.00 and a minimum of -8.02. The mean autofluorescence intensity in the 12-month wildtype sample was 45.19 ± 50.42, and 146.88 ± 66.80 in the age-matched *Abca4-/-* samples. The highest pixel intensity of the mutant was 235.87, and the lowest was 85.46. The maximum and the minimum autofluorescence intensity in the 12-month wildtype sample were 104.23 and -1.19, respectively (Figure 10B).

According to Tukey's HSD, none of the differences in mean autofluorescence level among the 6-month experimental genotypes was significant. The p-values were all above the 0.05 threshold. Hence, we did not observe the disease phenotype in our six-month *Abca4* null mice. However, the p-value of the difference in the autofluorescence levels between the 12-month *Abca4-/-* mice and the age-matched wildtype was 0.051. This implies that lipofuscin deposition was noticeably different between the two age-matched genotypes, but the sample size was too small to report a significant difference (n=4). The reported p-value between the six-month *Abca4-/-* mice and the 12-month *Abca4-/-* mice used for autofluorescence assay only was

p = 0.023 indicating that the amount of lipofuscin had significantly increased in the 12-month *Abca4* null mice.

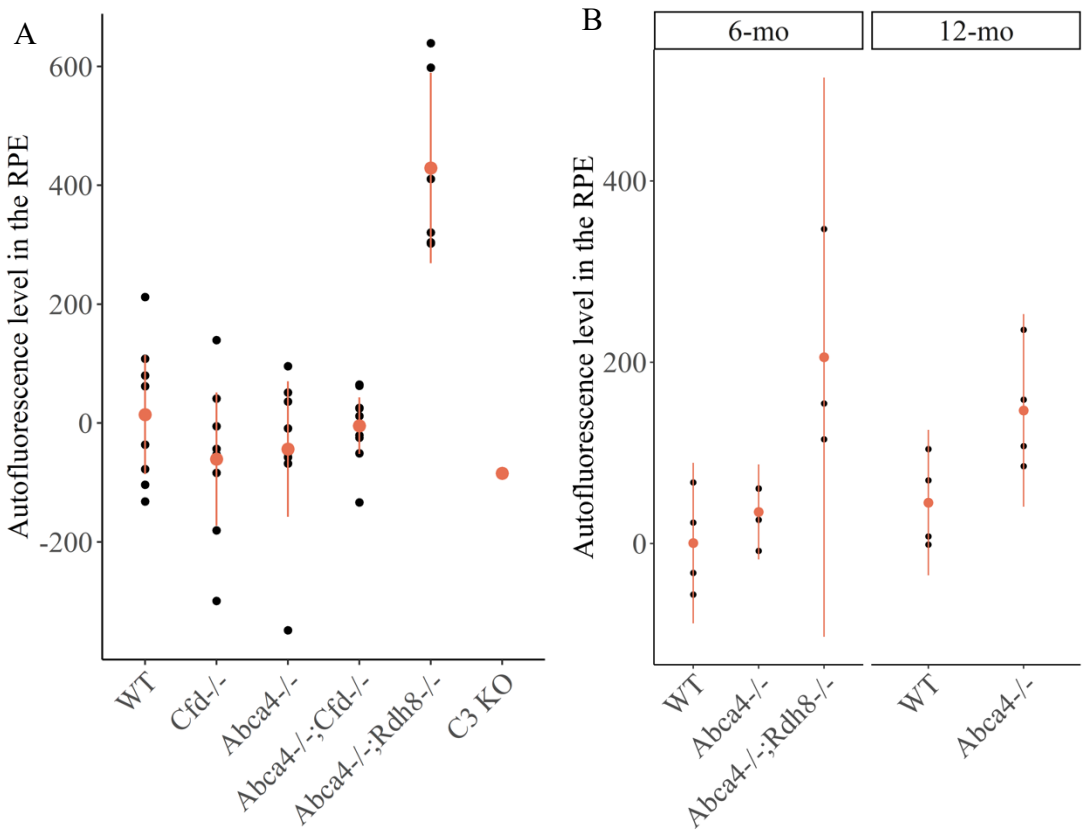

Figure 10. The autofluorescence levels in the RPE of mouse tissue sections. Panel A shows the autofluorescence levels in the six-month mouse tissue sections used for both the autofluorescence and the immunofluorescence assays (n=8). Background subtraction was performed when calculating the autofluorescence levels in the RPE. The background autofluorescence levels were calculated by averaging the autofluorescence levels in the ONL and INL of each individual, and they were subtracted from the total autofluorescence in the RPE. *Abca4-/-; Rdh8-/-* was used as the positive control, and C3 knockout (KO) was used as the negative control. Panel B shows the autofluorescence levels in the six-month and the 12-month mouse tissue sections used for autofluorescence assay only (n=4). The background autofluorescence levels were calculated using the autofluorescence levels in the sclera and subtracted from the total RPE autofluorescence levels. *Abca4-/-; Rdh8-/-* was the positive

control. Each black dot on both panels represents one individual and is the mean pixel intensity calculated using eight images collected. Four images were collected at the superior location of the retina, and four were collected at the inferior locations. The red dots are the mean autofluorescence levels calculated using the individuals with the same genotype, and the line marks the 95% confidence interval of each genotype.

3.3 Immunofluorescence in 6-month mice

The *Abca4-/-; Cfd-/-* samples had the highest mean immunofluorescence intensity in the RPE: 422.36 ± 251.89. The mean immunofluorescence levels in the RPE were similar in the *Abca4-/-*, *Cfd-/-* and the wildtype samples: 249.08 ± 94.84, 264.83 ± 169.30, and 283.62 ± 198.22.

The maximum immunofluorescence intensity among the wildtype samples was 624.34, and the minimum was 64.82 which is also the lowest value among all the experimental samples. The highest immunofluorescence intensity reported in the *Cfd -/-* was 558.01; the lowest level was 93.92. The highest and lowest immunofluorescence intensity in *Abca4-/-* samples were 395.43 and 72.81, respectively. The maximum immunofluorescence intensity in *Abca4-/-; Cfd-/-* was 752.32. It was also the highest immunofluorescence intensity of all experimental samples and the minimum immunofluorescence intensity in *Abca4-/-; Cfd-/-* samples was 156.49 (Figure 11).

According to Tukey's HSD, the p values of the difference observed in the immunofluorescence levels between the experimental samples were above 0.05 indicating the insignificance of the difference. Since the disease phenotype was absent in the six-month experimental samples used for both the autofluorescence and the immunofluorescence quantifications, it is difficult to interpret the role CFD has in STGD.

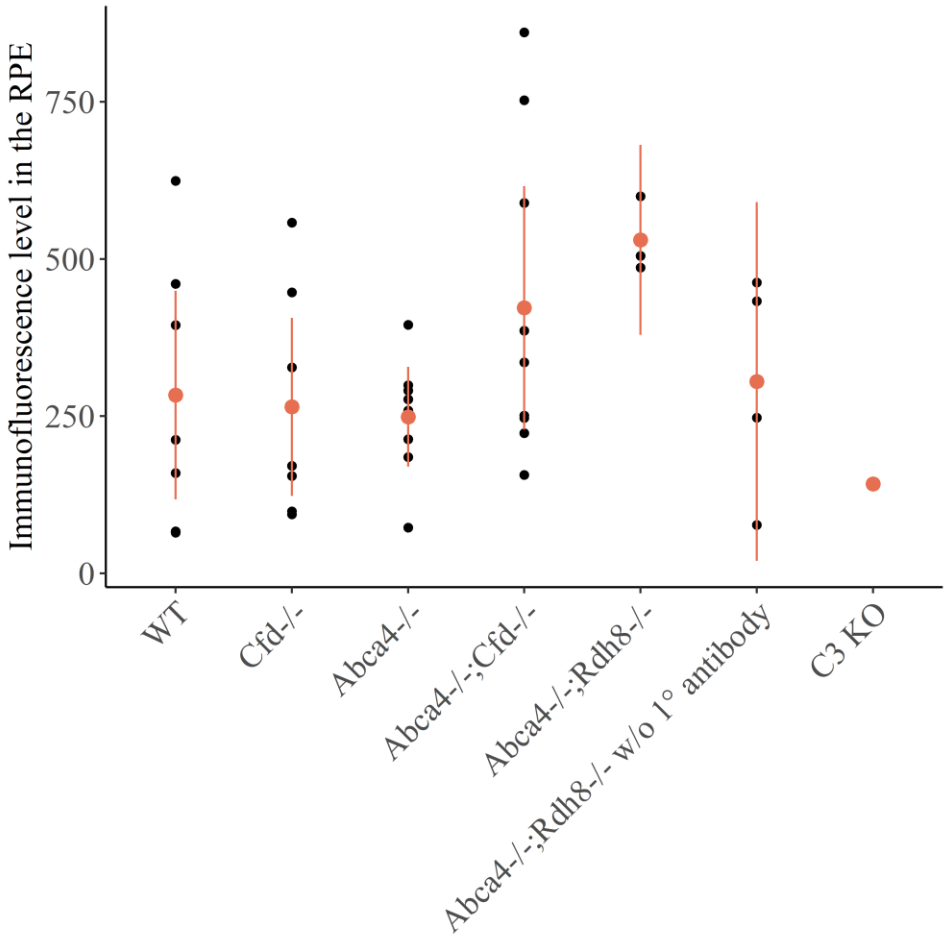

Figure 11. The immunofluorescence levels in the RPE of six-month mouse tissue sections. *Abca4-/-; Rdh8-/-* were used as positive control. Both *Abca4-/-; Rdh8-/-* without primary antibody and C3 KO were used as negative controls. Each black dot represents one individual (n=8) and is the mean immunofluorescence level calculated using eight images collected on one individual. Four images are collected on the superior side of the retina, and four are on the inferior side. The red dots are the mean immunofluorescence level calculated using the individuals with the same genotype, and the line marks the 95% confidence intervals of each genotype.

Chapter 4 Discussion

STGD is a recessive, heritable macular dystrophy caused by mutations in *ABCA4*. ABCA4 is a flippase found on the membrane of the photoreceptor outer disc segments and the

endolysosomes in the RPE, and it is responsible for correcting the orientation of *N-t*-R-PE so RDH8 can oxidize the compound and maintain the proper functionality of the visual cycle. Mutations in *ABCA4* slow down the removal of *N-t*-R-PE, which will undergo secondary condensation and produce lipofuscin. Lipofuscin is a toxic compound that can activate the complement system and cause damage to the RPE cells. It can be measured indirectly using fluorescent microscopy since it contains A2E, one of its major fluorophores with maximal excitation at 488 nm wavelength. The activation of the complement system in the RPE requires CFD. Hence, I measured the immunofluorescence level to indicate the amount of C3 accumulated in the RPE, with more C3 accumulated resulting in greater immunofluorescence. Change in C3 can assist us in gaining more knowledge about how CFD affects the progression of STGD.

4.1 Autofluorescence

The mean autofluorescence level in the six-month *Abca4-/-* samples was lower than the wildtype when the samples were used for both the autofluorescence and the immunofluorescence assays, contrasting with our prediction. However, the mean autofluorescence level in six-month *Abca4-/-* samples was higher than the wildtype when the samples were used for the autofluorescence assay only. The same trend was also noticed in the 12-month samples, as predicted.

The disease phenotype appeared to be absent in the six-month *Abca4-/-* samples (Figure 10). The hybrid mouse strain we used may be less susceptible resulting a later manifestation of the disease phenotype.

Different treatments applied to the tissue sections may contribute to the difference in the RPE autofluorescence level in the genotype- and age-matched experimental samples shown in

Figure 10. The slides used for the combined assay underwent AR and were incubated in solution containing Triton. The additional treatments may introduce variations in the autofluorescence level and cause the discrepancy observed in the same genotype (*Abca4* null or wildtype) at the same age.

Almost all the mean autofluorescence levels were below zero in the experimental samples used for both the autofluorescence and the immunofluorescence assays, except the wildtype. This can be due to the background used not being the ideal representative for the general tissue. Red blood cells also autofluorescence; thus, the red blood cells in either the ONL or the INL may inflate the autofluorescence level in these tissues, resulting in the calculated background autofluorescence level being higher than the actual value. When using the autofluorescence level in the sclera as the background autofluorescence level, the RPE autofluorescence levels after background subtraction were all above zero (Figure 10B).

In the study conducted by Charbel Issa et al. (2013), they observed an increase in the 488 nm autofluorescence level in *Abca4-/-* mice between three, six, and nine months, which is consistent with what we detected between the six- and 12-month *Abca4-/-* mouse samples used only for the autofluorescence assay.

However, the progress of lipofuscin accumulation in our study was slower than in other studies (Lenis et al., 2018; Radu et al., 2011). Radu et al. (2011) detected differences in the lipofuscin levels in the RPE between the wildtype mice and the albino *Abca4-/-* mice as young as two months. Lenis et al. (2018) also observed a significant increase in the total lipofuscin in the three-month albino *Abca4-/-* mice compared to the albino wildtype mice and the pigmented wildtype mice ($p=0.0186$ for both comparisons). The mice used may explain the late phenotypic manifestation in our study. We used pigmented mutated mice, yet the mutated mice in both cited

studies were albino. Melanin within the RPE protects cells against oxidative damage (Schütze et al., 2014). Albino mice lacking melanin are more susceptible to the damage caused by light, resulting in an earlier manifestation of the disease phenotype.

Dr. B. Ryan in the Chow lab has observed a higher mean autofluorescence level in 12-month pigmented *Abca4-/-* mice compared to the age-matched wildtype with a p-value less than 0.0001 using flat-mounted tissue (personal communication). This is consistent with what I observed using PFA-fix paraffin-embedded cross-section tissue. The p-value reported in my experiment was 0.051, which was right at the threshold of 0.05. The sample size I used (n=4) could be too small to generate a p-value less than 0.05. In addition, the mean autofluorescence level detected in the six-month *Abca4* null mice using the whole eye cup was higher than what was detected using cross-section tissue (approximately 100 versus 34.95). The tissue used for imaging may contribute to such a gap in observation. As in the studies conducted by Lenis et al. (2018) and Radu et al. (2011), Dr. B. Ryan used whole eye cups to collect images for the autofluorescence level measurement. This method captures the lipofuscin existing in the RPE of the whole eye. However, the cross sections I used were only 4 μm thick and could only reflect regional lipofuscin buildup in the RPE. The tissue used in flat-mount also underwent fewer processes than the PFA-fixed paraffin-embedded sections. For example, AR was performed in the slides used for both the autofluorescence and the immunofluorescence assays. Although AR amplifies the autofluorescence level among the cross-section tissue slides, such process may reduce the autofluorescence intensity in the cross-section tissue compared to the flat mount. Due to the above considerations, PFA-fixed paraffin-embedded section is not ideal for detecting autofluorescence in the RPE. Thus, flat-mounted tissue should be used when examining the deposition of lipofuscin in the *Abca4-/-* mouse RPE.

4.2 Immunofluorescence

The mean immunofluorescence levels in the RPE were similar among wildtype, *Cfd-/-*, and *Abca4-/-* samples. This indicates that the amount of C3 and its breakdown products are at a baseline level. The baseline level is above zero because the complement system is always activated at a low level via the AP (Xu & Chen, 2016). The unchanged amount of C3 observed across the three genotypes mentioned above indicates that the complement system was not fully activated. This may be due to the absence of the disease phenotype in the mutant. A study conducted by Williams et al., 2016 reported that when CFD was lost, the accumulation of C3 increased in the RPE while the breakdown product of C3 decreased. Because the alpha chain recognized by the antibody I used exists in C3 and some of its breakdown products, it is challenging to identify if the compound detected in the *Cfd-/-* samples is C3 or its breakdown products. The minor increase in C3 in the *Abca4-/-; Cfd-/-* samples shown in Figure 11 may be due to the increase in C3 accumulation when CFD is absent, but the decrease in the breakdown product of C3 reported in the study mentioned above may not occur in the *Abca4-/-; Cfd-/-* samples resulting a higher overall C3 detected in the *Abca4-/-; Cfd-/-* samples. Studies may use 12-month mice to further explore the effect loss of CFD has on STGD since the disease phenotype is more likely to be present at this age.

4.3 Conclusion

This study aimed to investigate the development of STGD and the role of CFD in the complement system by examining the accumulation of lipofuscin and C3 in the RPE in six-month and 12-month *Abca4-/-* mice. Quantifications of autofluorescence and immunofluorescence in the RPE were used as indirectly measurements for lipofuscin and C3. The autofluorescence levels were consistent among six-month experimental genotypes. This

implies that the disease phenotype was absent in the six-month mutated mice. However, the autofluorescence level was significantly higher in the 12-month *Abca4-/-* mice than in the age-matched wildtype. This suggests that the accumulation of lipofuscin had increased in the 12-month *Abca4-/-* mice compared to the age-matched wildtype. In addition, the autofluorescence level in the 12-month mutated mice was higher than in the six-month mutated mice, indicating the buildup of lipofuscin in the RPE of the *Abca4-/-* mice increased significantly as the mice aged. Moreover, the accumulation of lipofuscin increased between six-month and 12-month *Abca4-/-* mice which was consistent with the observation using flat-mounted samples suggesting that PFA-fixed paraffin-embedded tissue sections may be a convenient alternative to study the role of CFD in STGD.

The amount of C3 detected in the RPE remained unchanged across the experimental genotypes, as indicated by the consistency in the immunofluorescence level measured in the RPE. This suggests that the complement system was not wholly activated in the experimental samples. As a result, the role of CFD cannot be evaluated.

References

Allikmets, R., Singh, N., Sun, H., Shroyer, N. F., Hutchinson, A., Chidambaram, A., Gerrard, B., Baird, L., Stauffer, D., Peiffer, A., Rattner, A., Smallwood, P., Li, Y., Anderson, K. L., Lewis, R. A., Nathans, J., Leppert, M., Dean, M., & Lupski, J. R. (1997). A photoreceptor cell-specific ATP-binding transporter gene (*ABCR*) is mutated in recessive Stargardt macular dystrophy. *Nature Genetics*, *15*(3), 236–246. https://doi.org/10.1038/ng0397-236

Barratt, J., & Weitz, I. (2021). Complement factor D as a strategic target for regulating the alternative complement pathway. *Frontiers in Immunology*, *12*(September), Article September. https://doi.org/10.3389/fimmu.2021.712572

Boyer, D. S., Schmidt-Erfurth, U., van Lookeren Campagne, M., Henry, E. C., & Brittain, C. (2017). The pathophysiology of Geographic atrophy secondary to age-related macular degeneration and the compliment pathway as a therapeutic target. *Retina*, *37*(5), Article 5. https://doi.org/10.1097/IAE.0000000000001392

Burke, T. R., Duncker, T., Woods, R. L., Greenberg, J. P., Zernant, J., Tsang, S. H., Smith, R. T., Allikmets, R., Sparrow, J. R., & Delori, F. C. (2014). Quantitative fundus autofluorescence in recessive Stargardt disease. *Investigative Opthalmology & Visual Science*, *55*(5), 2841. https://doi.org/10.1167/iovs.13-13624

Charbel Issa, P., Barnard, A. R., Singh, M. S., Carter, E., Jiang, Z., Radu, R. A., Schraermeyer, U., & MacLaren, R. E. (2013). Fundus autofluorescence in the *Abca4-/-* mouse model of Stargardt disease-correlation with accumulation of A2E, retinal function, and histology. *Investigative Ophthalmology and Visual Science*, *54*(8), Article 8. https://doi.org/10.1167/iovs.13-11688

Croce, A. C., & Bottiroli, G. (2014). Autofluorescence spectroscopy and imaging: A tool for biomedical research and diagnosis. *European Journal of Histochemistry*. https://doi.org/10.4081/ejh.2014.2461

Davis, A. S., Richter, A., Becker, S., Moyer, J. E., Sandouk, A., Skinner, J., & Taubenberger, J. K. (2014). Characterizing and diminishing autofluorescence in formalin-fixed paraffin-embedded human respiratory tissue. *Journal of Histochemistry & Cytochemistry*, *62*(6), 405–423. https://doi.org/10.1369/0022155414531549

D'Ambra-Cabry, K., Deng, D. H., Flynn, K. L., Magee, K. L., & Deng, J.-S. (1995). Antigen retrieval in immunofluorescent testing of bullous pemphigoid: *The American Journal of Dermatopathology*, *17*(6), 560–563. https://doi.org/10.1097/00000372-199512000-00006

Héja, D., Kocsis, A., Dobó, J., Szilágyi, K., Szász, R., Závodszky, P., Pál, G., & Gál, P. (2012). Revised mechanism of complement lectin-pathway activation revealing the role of serine protease MASP-1 as the exclusive activator of MASP-2. *Proceedings of the National Academy of Sciences*, *109*(26), 10498–10503. https://doi.org/10.1073/pnas.1202588109

Kefalov, V. J. (2012). Rod and cone visual pigments and phototransduction through pharmacological, genetic, and physiological approaches. *Journal of Biological Chemistry*, *287*(3), 1635–1641. https://doi.org/10.1074/jbc.R111.303008

Kolb, H. (1995). Photoreceptors. In H. Kolb, E. Fernandez, & R. Nelson (Eds.), *Webvision: The Organization of the Retina and Visual System*. University of Utah Health Sciences Center. http://www.ncbi.nlm.nih.gov/books/NBK11522/

Lenis, T. L., Hu, J., Ng, S. Y., Jiang, Z., Sarfare, S., Lloyd, M. B., Esposito, N. J., Samuel, W., Jaworski, C., Bok, D., Finnemann, S. C., Radeke, M. J., Redmond, T. M., Travis, G. H., & Radu, R. A. (2018). Expression of ABCA4 in the retinal pigment epithelium and its implications for Stargardt macular degeneration. *Proceedings of the National Academy of Sciences*, *115*(47). https://doi.org/10.1073/pnas.1802519115

Molday, R. S., Garces, F. A., Scortecci, J. F., & Molday, L. L. (2022). Structure and function of ABCA4 and its role in the visual cycle and Stargardt macular degeneration. *Progress in Retinal and Eye Research*, *89*, 101036. https://doi.org/10.1016/j.preteyeres.2021.101036

Perusek, L., & Maeda, T. (2013). Vitamin A derivatives as treatment options for retinal degenerative diseases. *Nutrients*, *5*(7), 2646–2666. https://doi.org/10.3390/nu5072646

Purves, D., & Williams, S. M. (Eds.). (2001). *Neuroscience* (2. ed). Sinauer Associates.

Radu, R. A., Hu, J., Yuan, Q., Welch, D. L., Makshanoff, J., Lloyd, M., McMullen, S., Travis, G. H., & Bok, D. (2011). Complement system dysregulation and inflammation in the retinal pigment epithelium of a mouse model for Stargardt macular degeneration. *Journal of Biological Chemistry*, *286*(21), Article 21. https://doi.org/10.1074/jbc.M110.191866

Rehman, I., Hazhirkarzar, B., & Patel, B. C. (2024). Anatomy, head and neck, eye. In *StatPearls*. StatPearls Publishing. http://www.ncbi.nlm.nih.gov/books/NBK482428/

Saari, J. C. (2012). Vitamin A metabolism in rod and cone visual cycles. *Annual Review of Nutrition*, *32*(1), 125–145. https://doi.org/10.1146/annurev-nutr-071811-150748

Schütze, C., Ritter, M., Blum, R., Zotter, S., Baumann, B., Pircher, M., Hitzenberger, C. K., & Schmidt-Erfurth, U. (2014). Retinal pigment epithelium findings in patients with Albinism using wide-field polarization-sensitive optical coherence tomography. *Retina*, *34*(11), 2208–2217. https://doi.org/10.1097/IAE.0000000000000224

Scortecci, J. F., Molday, L. L., Curtis, S. B., Garces, F. A., Panwar, P., Van Petegem, F., & Molday, R. S. (2021). Cryo-EM structures of the ABCA4 importer reveal mechanisms underlying substrate binding and Stargardt disease. *Nature Communications*, *12*(1), 5902. https://doi.org/10.1038/s41467-021-26161-7

Simó, R., Villarroel, M., Corraliza, L., Hernández, C., & Garcia-Ramírez, M. (2010). The retinal pigment epithelium: something more than a constituent of the blood-retinal barrier—implications for the pathogenesis of diabetic retinopathy. *Journal of Biomedicine and Biotechnology*, *2010*, 1–15. https://doi.org/10.1155/2010/190724

Weng, J., Mata, N. L., Azarian, S. M., Tzekov, R. T., Birch, D. G., & Travis, G. H. (1999). Insights into the function of rim protein in photoreceptors and etiology of Stargardt's disease from the phenotype in *abcr* knockout mice. *Cell*, *98*(1), 13–23. https://doi.org/10.1016/S0092-8674(00)80602-9

Williams, J. A. E., Stampoulis, D., Gunter, C. E., Greenwood, J., Adamson, P., & Moss, S. E. (2016). Regulation of C3 activation by the alternative complement pathway in the mouse retina. *PLoS ONE*, *11*(8), Article 8. https://doi.org/10.1371/journal.pone.0161898

Wu, Y., Fishkin, N. E., Pande, A., Pande, J., & Sparrow, J. R. (2009). Novel lipofuscin bisretinoids prominent in human retina and in a model of recessive Stargardt disease. *Journal of Biological Chemistry*, *284*(30), 20155–20166. https://doi.org/10.1074/jbc.M109.021345

Xu, H., & Chen, M. (2016). Targeting the complement system for the management of retinal inflammatory and degenerative diseases. *European Journal of Pharmacology*, *787*, 94–104. https://doi.org/10.1016/j.ejphar.2016.03.001

Xu, Y., Ma, M., Ippolito, G. C., Schroeder, H. W., Carroll, M. C., & Volanakis, J. E. (2001). Complement activation in factor D-deficient mice. *Proceedings of the National Academy of Sciences of the United States of America*, *98*(25), Article 25. https://doi.org/10.1073/pnas.261428398

Zhou, J., Jang, Y. P., Kim, S. R., & Sparrow, J. R. (2006). Complement activation by photooxidation products of A2E, a lipofuscin constituent of the retinal pigment epithelium. *Proceedings of the National Academy of Sciences*, *103*(44), 16182–16187. https://doi.org/10.1073/pnas.0604255103